A 60-Heme Reductase Complex from an Anammox Bacterium Shows an Extended Electron Transfer Pathway

Authors

Andreas Dietl[a], Wouter J. Maalcke[b], Christina Ferousi[b,1], Mike S.M. Jetten[b], Boran Kartal[b,2] and Thomas R.M. Barends[a]*

[a]Department of Biomolecular Mechanisms, Max Planck Institute for Medical Research, Jahnstrasse 29, Heidelberg, 69120, Germany

[b]Department of Microbiology, Radboud University, Heyendaalseweg 135, Nijmegen, 6525AJ, The Netherlands

Correspondence email: thomas.barends@mpimf-heidelberg.mpg.de

[1] Current address: Department of Chemistry and Chemical Biology, Cornell University, Ithaca, NY 14853

[2] Current address: Microbial Physiology Group, Max Plank Institute for Marine Microbiology, Bremen, Germany

Synopsis

The heterododecameric complex of a reducing octaheme cytochrome *c* with its redox partner shows an extended electron transfer pathway.

Abstract

The hydroxylamine oxidoreductase/hydrazine dehydrogenase (HAO/HDH) protein family constitutes an important group of octaheme cytochromes *c* (OCCs). The majority of these proteins form homotrimers with their subunits being covalently attached to each other *via* a rare crosslink between the catalytic heme moiety and a conserved tyrosine residue of an adjacent subunit. This covalent crosslink has been proposed to modulate the active site heme towards oxidative catalysis by distorting the heme plane. In this study, we determined the crystal structure of a stable complex of a HAO homologue (KsHAOr) with its diheme cytochrome *c* redox partner (KsDH) from the anammox bacterium *Kuenenia stuttgartiensis*. KsHAOr lacks the tyrosine crosslink and is therefore tuned to reductive catalysis. The molecular model of the KsHAOr-DH complex at 2.6 Å resolution shows a heterododecameric ($\alpha_6\beta_6$) assembly which was also shown to be the oligomeric state in solution by analytical ultracentrifugation and multi-angle static light scattering. The 60-heme-containing protein complex reveals a unique extended electron transfer pathway and gives deeper insights into catalysis and electron transfer in reductive OCCs.

Keywords: Hydroxylamine oxidoreductase, anaerobic ammonium oxidation, electron transfer.

1. Introduction

Anaerobic ammonium-oxidizing (anammox) bacteria are chemolithoautotrophic microorganisms that make a living by oxidizing ammonium with nitrite as terminal electron acceptor yielding nitrogen gas and water (see (Kartal *et al.*, 2013) for a review). This process involves nitric oxide (NO) and hydrazine (N_2H_4) as free intermediates (Kartal *et al.*, 2011). Most key biochemical reactions in the anammox pathway are catalysed by multiheme cytochromes *c* (MCCs), which are crucial players in microbial energy conversion. Octaheme *c*-type cytochromes (OCCs) form a broad class of MCCs with diverse functions in nitrogen and sulfur metabolism (Simon *et al.*, 2011). The hydroxylamine oxidoreductase/hydrazine dehydrogenase (HAO/HDH) protein family constitutes an important group of OCCs next to the octaheme nitrite and tetrathionate reductases (ONRs and OTRs, respectively) (Mowat *et al.*, 2004, Atkinson *et al.*, 2007, Polyakov *et al.*, 2009, Tikhonova *et al.*, 2006). Most representatives of the HAO/HDH family catalyze reactions in the oxidative direction whereas members of the ONR/OTR family are tuned to reductive catalysis (Klotz *et al.*, 2008).

The genomes of anammox bacteria encode a broad variety of OCCs belonging to the HAO/HDH family. These include hydrazine dehydrogenase (HDH), which oxidizes hydrazine to dinitrogen gas (Maalcke *et al.*, 2016) as well as hydroxylamine oxidase (HOX), converting hydroxylamine into nitric oxide (Maalcke *et al.*, 2014). Despite relatively low amino acid sequence identities, both enzymes possess several

common structural features with the prototypical representative of the HAO/HDH family, the hydroxylamine oxidoreductase from *Nitrosomonas europaea* (NeHAO), a central enzyme in the bacterial aerobic ammonia oxidation pathway (Igarashi *et al.*, 1997, Cedervall *et al.*, 2013). HAO/HDH family members typically form homotrimeric assemblies, where the monomers exhibit several conserved (mostly α-helical) secondary structural elements and possess eight heme-binding motifs ($CX_{2-4}CH$, reviewed in (Klotz *et al.*, 2008)). Importantly, the structural arrangement of these covalently bound hemes *c*, which are commonly numbered by the appearance of their heme binding motifs along the sequence, is highly conserved in all members of the family, and gives rise to an interconnected electron transfer system.

Of the eight hemes, heme 1 is located on the outside of this ring-like heme arrangement close to the protein surface and was therefore proposed to be an electron exit site in NeHAO from where electrons released during catalysis could be transferred to a redox partner (Igarashi *et al.*, 1997, Cedervall *et al.*, 2013). However, to our knowledge, no structure of a complex of an OCC with a redox partner protein has been reported so far.

Heme 4, which has a vacant distal coordination site, constitutes the active center whereas the other seven hemes are hexacoordinated (mostly His/His, but also His/Met and His/Lys) and are involved in electron transfer towards or away from the active site heme. Crystal structures of two oxidative HAO/HDH family members, *Nitrosomonas europaea* hydroxylamine oxidoreductase (NeHAO) (Igarashi *et al.*, 1997, Cedervall *et al.*, 2013) and *Kuenenia stuttgartiensis* hydroxylamine oxidase (KsHOX) (Maalcke *et al.*, 2014) revealed a unique covalent crosslink between the catalytic heme 4 and a tyrosine residue from an adjacent subunit in the trimer. The presence of this crosslink results in a pronounced deformation of the active site heme plane known as “ruffling” (Jentzen *et al.*, 1998, Jentzen *et al.*, 1997, Shelnutt *et al.*, 1998), leading to a lowering of its redox potential (Fernández *et al.*, 2008, Kleingardner *et al.*, 2018, Kleingardner & Bren, 2015, Liptak *et al.*, 2010). The tyrosine involved in the active site heme crosslink is highly conserved within members of the HAO/HDH family and is considered a hallmark of oxidative OCCs (Klotz *et al.*, 2008).

By contrast, another HAO/HDH homologue isolated from the anammox bacterium *Kuenenia stuttgartiensis*, KsHAOr (the gene product of kustc0458), lacks this tyrosine crosslink and is therefore tuned to reductive catalysis (Kartal *et al.*, 2013). More importantly, this protein was co-purified with its physiological redox partner, the diheme cytochrome *c* KsDH (the gene product of kustc0457), with which it forms a stable complex.

Given its reductase-type active site heme, KsHAOr-DH has been suggested to function as a nitrite reductase in *Kuenenia* (Kartal *et al.*, 2013). Interestingly, while the reduction of nitrite to NO is central to the anammox metabolism, various anammox organisms appear to have different enzymes for this

purpose. In the anammox bacterium *Jettenia caeni,* this reaction is catalyzed by a copper-containing nitrite reductase (Cu-NIR) (Hira *et al.*, 2012, Ali *et al.*, 2015) whereas in another anammox organism, *Scalindua* (van de Vossenberg *et al.*, 2013) the *cd*$_1$ heme-containing (*cd*$_1$-NIR) NirS is expressed predominantly. A *cd*$_1$-NIR homologue is also present in *Kuenenia* (Strous *et al.*, 2006, Kartal *et al.*, 2011) but is expressed at a lower level. Strikingly, genomes of the anammox genus *Brocadia* encode neither Cu-NIR nor *cd*$_1$-NIR homologues (Oshiki *et al.*, 2016) but do posess orthologues of KsHAOr. As is the case for the pentaheme cytochrome *c* nitrite reductase NrfA (Einsle *et al.*, 2000), most of the investigated reductive OCCs such as *T. nitratireducens* ONR (Tikhonova *et al.*, 2006) or εHAOs (Haase *et al.*, 2017) fully reduce nitrite and hydroxylamine to ammonium. An exception is the enzyme *I. hospitalis* IhHAO (Parey *et al.*, 2016) which has been shown to generate NO from the aformentioned substrates *in vitro* while ammonium or hydroxylamine (from the reduction of nitrite) could not be detected. Thus, whether the KsHAOr-DH complex plays a role in nitrite reduction in *Kuenenia* is unclear at the moment and requires detailed biochemical studies.

Here we report the structural and biophysical characterization of the KsHAOr-DH complex. The crystal structure of this complex shows a unique heterododecameric assembly and reveals two copies of a unique extended electron transfer pathway of 30 hemes each. The structural model provides deeper insights into catalysis and electron transfer in reductive OCCs.

2. Materials and Methods

2.1. Protein purification

The KsHAOr-DH (kustc0457-58) complex was purified from *Kuenenia stuttgartiensis* as described for other OCCs in (Kartal *et al.*, 2011) by a two-step procedure using anion-exchange and hydroxyapatite chromatography. The identification of the components of the KsHAOr-DH complex by MALDI-TOF mass spectrometry as well as its detailed biochemical analysis will be described elsewhere.

For crystallization experiments, the buffer was exchanged by diafiltration in 30 kDa MWCO Amicon tubes (Millipore Bioscience, Schwalbach, Germany) against 25 mM KCl, 25 mM HEPES/KOH, pH 7.5. The concentrated protein solutions ($A_{280}^{1\ cm} \approx 0.2$ for a 1:100 dilution, $A_{409}/A_{280} \approx 3.5$) were divided into 50 µl aliquots, which were shock frozen in thin-walled PCR tubes in liquid nitrogen and stored at -80 °C. KsHAOr-DH samples used for AUC and SEC-MALS analyses were further purified by size exclusion chromatography using a Superose 6 (10/300 GL) column (GE Healthcare, Uppsala, Sweden) in a buffer containing 150 mM KCl, 50 mM HEPES/KOH pH 7.5 at a flow rate of 0.5 ml min^{-1} and 8 °C.

2.2. Analytical ultracentrifugation (AUC)

The oligomeric state of the KsHAOr-DH complex was investigated using both the sedimentation velocity (AUC-SV) and sedimentation equilibrium (AUC-SE) methods in a Proteome LabXL-I analytical ultracentrifuge equipped with an An-60 Ti rotor (Beckman Coulter Inc., Palo Alto, California, USA). An aliquot of protein stock solution was diluted in 25 mM KCl, 25 mM HEPES/KOH pH 7.5 and the buffer was equilibrated by repeated ultrafiltration in 30 kDa MWCO Amicon tubes (Millipore, Schwalbach, Germany). The final protein sample (400 µl) was adjusted to $A_{280}^{1\ cm} = 0.22$, $A_{409}^{1\ cm} = 0.65$ by dilution with the reference buffer (flow-through from the last ultrafiltration step) and sedimented in a flow-through 12 mm centerpiece at 20,000 rpm, 20 °C for 24 h. Absorption scan data were recorded at 280 and 409 nm. Sedimentation coefficient distributions c(S) were calculated using SEDFIT 12.44 (Schuck, 2000) assuming a partial specific volume of the protein of 0.7300 ml g^{-1} as well as buffer viscosity and density values of $1.0194 \cdot 10^{-2}$ g cm^{-1} s^{-1} and 1.00135 g cm^{-3}, respectively, as calculated using the program SEDNTERP 1.09 (Hayes D.B. et al., New Hampshire, USA). Molecular mass estimates were obtained assuming a fixed frictional ratio of 1.2. Theoretical sedimentation coefficients were calculated from the crystal structure using the program HYDROPRO 10 (García de la Torre *et al.*, 2000).

Sedimentation equilibrium measurements were carried out with the identical sample but with only 200 µl in the sample cell to minimize the time needed to reach equilibrium conditions. The KsHAOr-DH sample was equilibrated at 3,000 rpm, 6,000 rpm and 7,500 rpm for 22 h at 20 °C. The data points averaged from

five individual scans at 280 nm that showed meniscus depletion (6,000 and 7,500 rpm) were globally fitted assuming a model of discrete non-interacting species in SEDPHAT 10.55 (Schuck, 2000).

2.3. Size exclusion chromatography and multi-angle static light scattering (SEC-MALS)

The KsHAOr-DH complex was further analyzed by analytical size exclusion chromatography (SEC) at a flow rate of 0.5 ml min^{-1} using a Waters HPLC system (Waters Corp., Milford, Massachusetts, USA), equipped with a Superdex 200 increase (10/300 GL) column (GE Healthcare, Uppsala, Sweden), a UV-Vis and a refractive index (RI) detector. Prior to the experiments, the column had been pre-equilibrated with gel filtration buffer (150 mM KCl, 50 mM HEPES/KOH, pH 7.5) at room temperature. 40 µl protein sample (approximately 180 µg) was injected using an autosampler and absorbance traces were monitored at 280 and 409 nm. Multi-angle static light scattering (MALS) analysis was performed in line using a DAWN HELEOS multi-angle scattered light photometer (Wyatt Technology Corp., Santa Barbara, USA). Data were processed using the ASTRA 6.1.1 software assuming a refractive index increment of 0.185 mL g^{-1}.

2.4. Crystallization

Initial crystallization screening was performed using a Mosquito crystallization robot (TTP Labtech, Melbourne, UK) at 20°C against commercial screens that had been pipetted into 96-well sitting-drop trays (Greiner XTL low-profile, Greiner Bio One, Frickenhausen, Germany). 100 nL of protein ($A_{280}^{1cm} \approx 0.2$ for a 1:100 dilution) was mixed with 100 nL of reservoir solution. Initial crystals grew within three weeks from 1.5-2.0 M ammonium sulfate and 0-15% (v/v) glycerol as tiny rhombohedra of 15 × 10 × 10 µm. For optimization of the crystallization conditions, hanging drop vapor diffusion experiments were set up by mixing 1-2 µl KsHAOr-DH protein stock with an equal volume of reservoir solution, followed by equilibration against 800 µl of reservoir solution at 293 K. Dark red, rhombic crystals (100×100×50 µm) of the KsHAOr-DH complex grew within five days when 1.5 M ammonium sulfate, 1% (v/v) Tween-20 was used as precipitant. Crystals were cryoprotected by soaking for 1-5 minutes in 1.5 M ammonium sulfate supplemented with 25% (v/v) ethylene glycol followed by flash-cooling in liquid nitrogen.

2.5. Data collection and structure solution

Two datasets were collected: a highly redundant 3.7 Å resolution dataset at the iron K-edge peak wavelength of 1.7 Å collected at beam line X10SA of the Swiss Light Source (Villigen, Switzerland) and a 2.6 Å resolution dataset collected at a wavelength of 1.54 Å on a MicroMax 007HF rotating anode (Rigaku) equipped with a MAR345 image plate. Unfortunately, a higher resolution than 2.6 Å could not be obtained using a synchrotron source. All data were collected at 100 K and processed using XDS

(Kabsch, 2010). Phasing was performed by AutoSHARP (Vonrhein *et al.*, 2007) using the highly redundant peak wavelength data, resulting in a readily interpretable map ($FOM_{acentric}$=0.3 before density modification) into which an initial model was built using COOT (Emsley & Cowtan, 2004). This was refined against the 2.6 Å resolution rotating anode data, initially by simulated annealing using PHENIX (Adams *et al.*, 2010), followed by restrained refinement with REFMAC5 (Murshudov *et al.*, 2011), and finally again with PHENIX (Adams *et al.*, 2010). Data collection and model statistics are reported in Tables 1 and 2, respectively.

3. Results

3.1. Quaternary structure of the KsHAOr-DH complex

The crystal structure of the KsHAOr-DH complex was determined at a resolution of 2.6 Å (Table 1 and 2). The asymmetric unit contains one chain each of the octaheme *c*-type cytochrome KsHAOr (kustc0458, α-subunit) and the diheme cytochrome *c* KsDH (kustc0457, β-subunit). An $\alpha_6\beta_6$ heterododecamer is formed by the crystallographic symmetry operators, consisting of two tulip bulb-shaped KsHAOr trimers held together by an equatorial ring of three KsDH dimers (Figure 1). The dimensions of the heterododecamer are ~190 Å in length and ~110 Å in equatorial diameter, the buried surface area formed by all the interfaces together is 129,763 $Å^2$. A large, open cavity is formed between the two oppositely oriented KsHAOr trimers. This assembly, which the PISA software (Krissinel & Henrick, 2004) estimated to be stable in solution, has a calculated mass of 545.8 kDa and contains 60 covalently bound heme groups.

The occurrence of this assembly in solution is consistent with results obtained by sedimentation velocity analytical ultracentrifugation, which showed a single species with an $S_{w,20}$ value of 18.5 S (Figure S1). This is in excellent agreement with the sedimentation coefficient calculated for the heterododecamer by HYDROPRO (García de la Torre *et al.*, 2000) of $S_{w,20}$=18.7 S. Moreover, the maximum sedimentation coefficient ($S_{max} \approx 0.00361 \times M^{2/3}$) calculated for a perfect sphere of this molecular weight is 24.3 S, resulting in an $S_{max}/S_{w,\ 20}$ ratio of 1.3, which is consistent with the elongated shape of the assembly (Erickson, 2009). Sedimentation equilibrium analysis (Figure S2) resulted in a molecular mass of 545,974 Da, which is also consistent with the $\alpha_6\beta_6$ complex observed in the crystal (calculated mass 545,883 Da).

In addition, size exclusion chromatography coupled with multi-angle static light scattering (SEC-MALS) showed a single peak at an elution volume of 10.3 ml. The molecular mass of the material eluting in this peak as determined by MALS analysis was 570.4 ± 2.9 kDa (Figure S3).

3.2. The KsHAOr-DH heterododecamer shows two extended networks of 30 heme groups each

Each KsHAOr subunit harbours seven bis-histidine coordinated *c*-type hemes (hemes 1, 2, 3, 5, 6, 7 and 8) in addition to the active site heme 4 which is His/water-coordinated. Like in other trimeric OCCs this establishes a ring-like arrangement of 24 hemes connecting hemes 2 and 8 of adjacent monomers. The 24 hemes in the KsHAOr trimer are fully superimposable with those from NeHAO and KsHOX. Both hemes in the KsDH subunit are His/Met ligated. In the KsHAOr-DH complex the heme *c* bound to the N-terminal heme binding motif (heme 1') from each KsDH subunit is positioned next to heme 1 of KsHAOr (edge-to-edge distance 7.5 Å (Moser *et al.*, 2008)), extending the electron transfer network of the HAOr heme ring (Figure 2). This results in a system of 30 electronically coupled heme cofactors within each of

the upper and lower halves of the heterododecamer. The distance between KsDH subunits belonging to the lower and upper half of the heterododecamer, however, is too large for single-step electron transfer (edge-to-edge distance ~30 Å).

3.3. Structure of the octaheme cytochrome *c* KsHAOr

The structural model of the octaheme *c*-type cytochrome KsHAOr includes 506 residues (Ile48 to Ser553), *i.e.* seven residues at the N-terminus after the predicted signal sequence cleavage site (Thr41) and one at the C-terminus (Lys554) are not resolved. KsHAOr is an entirely α-helical protein with a total of 21 well-defined helices. Although it shares only 21 % sequence identity with KsHOX and 26% with NeHAO its overall fold is highly similar. A structural alignment of the protein monomers results in a backbone rmsd of 1.5 Å to NeHAO (for 399 Cα atoms) and 1.8 Å to KsHOX (for 366 Cα atoms). In agreement with NeHAO and KsHOX, the KsHAOr monomer can be subdivided into an N-terminal domain N1 (residues 41 to 76), an N2 domain (77-275) and a central domain (276 to 553) (Figure 3, S4). The N1 domain of KsHAOr (residues 48 to 76 in the model) is not fully resolved but seems to adopt an orientation similar to the corresponding domain in NeHAO, whereas in KsHOX this domain is oriented differently. In contrast to NeHAO, a C-terminal domain extending α21b (α22b in NeHAO) is lacking completely. KsHAOr shows insertions of three short helices (α12, α18 and α19, Figure S4) missing in the NeHAO structure. Helices α18 and α19 are part of the extended loop connecting the long helices α17 and α20 (corresponding to α20 and α21 in NeHAO), which closes the catalytic pocket located above hemes 4, 6 and 7. The characteristic three-helix bundle at the C-terminus (Figure 3) is formed by two parallel helices (α17 and α21) and the antiparallel helix α20 (Figure S4), corresponding to the parallel helices α20 and α22, respectively, and the antiparallel helix α21 in NeHAO. The long C-terminal helix α21 is broken into two parts (α21a and α21b) by Pro527 similar as described for NeHAO, though the characteristic tyrosine necessary for the covalent crosslink to heme 4 is lacking in the sequence.

3.4. Active site of KsHAOr

The active site of KsHAOr (Figure 4a) is composed of heme 4 in close proximity to heme 6. Heme 4, which is accessible from the solvent through a broad, funnel-shaped entrance on the surface of the protein, is bound by the heme binding motif ($C^{236}DMC^{239}H^{240}$) originating from helix α10 with a distance of 2.0 Å between the proximal histidine 240 and the heme iron. As in oxidative HAO homologues, a conserved Asp-His pair (Asp274 and His275) is located in the loop connecting helices α12 and α13 on the distal face of heme 4. The position of the tyrosine forming the crosslink to heme 4 in NeHAO and KsHOX is occupied by Trp522', which is part of a conserved triple-tryptophan (WWW) motif in the loop separating helix α21a and α21b of the adjacent subunit. Additional electron density at the distal face of

the active site heme indicates a solvent molecule bound as the distal ligand of heme 4 (iron-oxygen distance 2.1 Å). The porphyrin plane of heme 4 is significantly less "ruffled" (Figure 4a) than is the case for the crosslinked hemes in KsHOX (Figure 4b) and NeHAO. Moreover, in KsHAOr heme 4 appears bent in the middle rather than ruffled, along the axis passing through the C20, Fe and C10 atoms.

The conserved Asp274 forms a hydrogen bond to the distal water ligand at a distance of 3.3 Å. Moreover, the Nε of Trp522' is in close proximity to the carboxyl group of Asp274 (nitrogen-oxygen distance 3.5 Å). The distance between His275 Nε and the water ligand is too large for a hydrogen bond (4.2 Å). A conserved methionine residue (Met341) is located in the distal pocket of the active site heme which is also present in KsHOX (Met323) but substituted by a tyrosine (Tyr358) in NeHAO.

3.5. Structure of the redox partner KsDH

The diheme cytochrome *c* KsDH is an α-helical protein with a total of six well defined helices (Figure 5, S5). The model includes 220 residues (Ile35 to Gln254), which means that the N-terminus in the structure is identical to the predicted signal sequence cleavage site (Ile35) and that six residues are not resolved at the C-terminal end. The protein structure can be subdivided into an N-terminal domain (residues 35 to 132), a flexible linker region (133-154) and a C-terminal domain (residues 155-254) (Figure 5, S5). The N- and C-terminal domains each have a heme *c* bound (heme 1' and heme 2', respectively) and consist of three helices (Figure 5). Two of the helices in each domain are oriented almost parallel to each other (α1 and α2, α4 and α5) and perpendicular to the third one (α3 and α6, respectively). Helix α3 is broken into two parts (α3a and α3b) by Pro128. The planes of the two hemes are related by a rotation of around 80°. Although the sequence identity between the N- and C-terminal domains is only 18% their structures can be superposed upon each other very well (backbone rmsd 1.4 Å). The structures of the individual domains also show high structural similarity with horse cytochrome *c* (pdb 1HRC, backbone rmsd 2.3 Å to the C-terminal domain, 2.6 Å to the N-terminal domain), which also bears a distal methionine ligand of the heme iron. However, horse cytochrome *c* contains insertions of two short helices (α2 and α4). The hydrophilic linker region assumes its stretched conformation by adopting a polyproline II (PPII) helix-like conformation in most regions as judged by Ramachandran analysis and indeed contains two proline-rich motifs (EPEP, PLRP).

4. Discussion

4.1. Structure of the KsHAOr-DH complex

The monomer of the octaheme *c*-type cytochrome KsHAOr shares high structural similarity with KsHOX (Maalcke *et al.*, 2014) and NeHAO (Igarashi *et al.*, 1997, Cedervall *et al.*, 2013), and forms conically shaped trimers as a part of the heterododecameric KsHAOr-DH complex. The KsHAOr-DH heterododecamer found in the crystal was also corroborated as the oligomeric form in solution by both AUC and SEC-MALS analyses. The N- and C-terminal domains of the diheme protein KsDH can each be seen as typical class 1 His/Met coordinated *c*-type cytochromes similar to mitochondrial cytochrome *c*. Given the close similarity between the two domains, it can be speculated whether this protein evolved by gene duplication of two identical monoheme cytochromes *c*. To our knowledge, the structure of the KsHAOr-DH heterododecamer is the first structural model of an octaheme *c*-type cytochrome in complex with a small redox partner, and displays a subunit arrangement that has not been described before. Besides acting as a redox partner, the KsDH molecules in the complex may aid in keeping the assembly of the two KsHAOr trimers together. The KsHAOr subunits within a trimer are not covalently linked. In contrast to the situation in the oxidizing OCCs KsHOX and NeHAO, there is no tyrosine mediating the covalent crosslink to heme 4 of an adjacent subunit but a conserved triple tryptophan (WWW) motif on a loop breaking the C-terminal helix. Moreover, the lack of the tyrosine crosslink likely accounts for the much less pronounced ruffling of the macrocycle plane of heme 4 and implies tuning of the enzyme towards reductive catalysis. The absence of the tyrosine-heme crosslink is consistent with other reductive OCCs such as *I. hospitalis* IhHAO (Parey *et al.*, 2016), εHAOs (Haase *et al.*, 2017), *T. nitratireducens* ONR (Polyakov *et al.*, 2009) or *W. succinogenes* MccA (Hermann *et al.*, 2015). However, other features present in some ONRs and also pentaheme cytochrome *c* nitrite reductases (NrfA; (Einsle *et al.*, 2000)), such as the CXXCK proximal active site heme binding motif or a conserved Ca^{2+}-binding site located above the catalytic heme are absent in KsHAOr.

4.2. Electron transfer within the KsHAOr-DH complex and from putative redox partners

The ring-like heme arrangement of each of the KsHAOr trimers in the KsHAOr-DH heterododecamer is identical to the situation in NeHAO and KsHOX and suggests a highly effective electron transport system between the active site heme 4 and the electron exchange site heme 1. Like in other trimeric OCCs, hemes 2, 3, 5, 6, 7 and 8 form a circular electron transport chain that extends throughout the trimer, connecting hemes 2 and 8 of adjacent monomers. The close proximity of heme 1 of KsHAOr to heme 1' of KsDH in the heterododecamer enables electron transfer between the two proteins. The observed docking site of KsDH near heme 1 of KsHAOr is also in agreement with the suspected interaction of NeHAO and its

redox partner cytochrome c_{554} (Igarashi *et al.*, 1997, Cedervall *et al.*, 2013). However, as this complex likely acts as a reductase, the electron flux must necessarily occur in a direction opposite to that in the substrate-oxidizing enzymes KsHOX and NeHAO, *i.e.*, electrons must be supplied by a redox partner that is currently unknown. However, the genes encoding KsHAOr (kustc0458) and KsDH (kustc0457) are closely colocalized with kustc0456, which encodes a putative cupredoxin-like protein, and which could be the physiological redox partner of KsHAOr-DH. Kustc0456, which is closely related to the blue copper protein amicyanin, would then bind to the side of a KsDH subunit and feed electrons to heme 2' at the surface of the complex (Figure 6). From KsDH the electrons would be transferred to the heme system of KsHAOr, where they are finally consumed for the reduction of its substrate at heme 4. This scenario is consistent with cd_1-type nitrite reductases, such as the one from *Paracocccus pantotrophus*, where pseudoazurin serves as electron donor and simultaneously facilitates the release of NO (Sam *et al.*, 2008). However, the genome of the anammox bacterium *Scalindua brodae* seems to lack a kustc0456 homologue, and the axial copper-coordinating methionine ligand present in all other *Kuenenia* cupredoxin paralogues is missing in kustc0456 as well as in its *Brocadia* and *Jettenia* orthologues.

In conclusion, the crystal structure and biophysical characterization of KsHAOr-DH presented here represents the first structure of a HAO-like protein in complex with a redox partner, and provides insights into the pathway for electrons into the protein. Moreover, the conformation of the active site heme is consistent with the proposed role of this complex as a nitrite reductase, a central function in anammox metabolism.

Acknowledgements

The authors wish to thank the X10SA beam line staff at the Swiss Light Source for their outstanding support and their excellent facility, and members of the Heidelberg/Dortmund data collection team for synchrotron data collection. We thank Chris Roome for excellent IT support. T.R.M.B. is very grateful to Ilme Schlichting for continuous support. The authors also thank Jan Keltjens for stimulating discussions.

Funding information

This work has been funded by the Max Planck society. MSMJ is supported by European Research Council (ERC Advanced Grant project EcoMoM 339880) and the SIAM Gravitation Grant on Anaerobic Microbiology (Netherlands Organization for Scientific Research, NWO/OCW gravitation SIAM 024.002 .002). BK is supported by the European Research Council (ERC Starting Grant GreenT 640422).

References

Adams, P. D., Afonine, P. V., Bunkoczi, G., Chen, V. B., Davis, I. W., Echols, N., Headd, J. J., Hung, L. W., Kapral, G. J., Grosse-Kunstleve, R. W., McCoy, A. J., Moriarty, N. W., Oeffner, R., Read, R. J., Richardson, D. C., Richardson, J. S., Terwilliger, T. C. & Zwart, P. H. (2010). *Acta Cryst. D* **66**, 213-221.

Ali, M., Oshiki, M., Awata, T., Isobe, K., Kimura, Z., Yoshikawa, H., Hira, D., Kindaichi, T., Satoh, H., Fujii, T. & Okabe, S. (2015). *Environ. Microbiol.* **17**, 2172-2189.

Atkinson, S. J., Mowat, C. G., Reid, G. A. & Chapman, S. K. (2007). *FEBS. Lett.* **581**, 3805–3808.

Cedervall, P., Hooper, A. B. & Wilmot, C. M. (2013). *Biochem.* **52**, 6211-6218.

DeLano, W. L. (2002). *The PyMOL Molecular Graphics System.*

Einsle, O., Stach, P., Messerschmidt, A., Simon, J., Kröger, A., Huber, R. & Kroneck, P. M. (2000). *J. Biol. Chem.* **275**, 39608–39616.

Emsley, P. & Cowtan, K. (2004). *Acta Cryst. D* **60**, 2126-2132.

Erickson, H. P. (2009). *Biolog. Proced. Online* **11**, 32-51.

Fernández, M. L., Estrin, D. A. & Bari, S. E. (2008). *J. Inorg. Biochem.* **102**, 1523–1530.

García de la Torre, J., Huertas, M. L. & Carrasco, B. (2000). *Biophys. J.* **78**, 719-730.

Gouet, P., Courcelle, E., Stuart, D. I. & Metoz, F. (1999). *Bioinformatics* **15**, 305-308.

Haase, D., Hermann, B., Einsle, O. & Simon, J. (2017). *Mol. Microbiol.* **105**, 127-138.

Hermann, B., Kern, M., La Pietra, L., Simon, J. & Einsle, O. (2015). *Nature* **520**, 706-U318.

Hira, D., Toh, H., Migita, C. T., Okubo, H., Nishiyama, T., Hattori, M., Furukawa, K. & Fujii, T. (2012). *FEBS. Lett.* **586**, 1658-1663.

Igarashi, N., Moriyama, H., Fujiwara, T., Fukumori, Y. & Tanaka, N. (1997). *Nat. Struct. Biol.* **4**, 276–284.

Jentzen, W., Ma, J. G. & Shelnutt, J. A. (1998). *Biophys. J.* **74**, 753–763.

Jentzen, W., Song, X.-Z. & Shelnutt, J. A. (1997). *J. Phys. Chem. B* **101**, 1684–1699.

Kabsch, W. (2010). *Acta Crystal D* **66**, 125-132.

Kartal, B., de Almeida, N. M., Maalcke, W. J., Op den Camp, H. J., Jetten, M. S. & Keltjens, J. T. (2013). *FEMS Microbiol. Rev.* **37**, 428-461.

Kartal, B., Maalcke, W. J., Almeida, N. M. d., Cirpus, I., Gloerich, J., Geerts, W., Op den Camp, H. J. M., Harhangi, H. R., Janssen-Megens, E. M., Francoijs, K.-J., Stunnenberg, H. G., Keltjens, J. T., Jetten, M. S. M. & Strous, M. (2011). *Nature* **479**, 127–130.

Kleingardner, J., Levin, B. D., Zoppellaro, G., Andersson, K. K., Elliott, S. J. & Bren, K. (2018). *J. Biol. Inorg. Chem*.

Kleingardner, J. G. & Bren, K. L. (2015). *Acc. Chem. Res.* **48**, 1845-1852.

Klotz, M. G., Schmid, M. C., Strous, M., den Camp, H., Jetten, M. S. M. & Hooper, A. B. (2008). *Environ. Microbiol.* **10**, 3150–3163.

Krissinel, E. & Henrick, K. (2004). *Acta Crystal. D* **60**, 2256-2268.

Liptak, M. D., Wen, X. & Bren, K. L. (2010). *J. Am. Chem. Soc.* **132**, 9753-9763.

Maalcke, W. J., Dietl, A., Marritt, S. J., Butt, J. N., Jetten, M. S., Keltjens, J. T., Barends, T. R. & Kartal, B. (2014). *J. Biol. Chem.* **289**, 1228-1242.

Maalcke, W. J., Reimann, J., de Vries, S., Butt, J. N., Dietl, A., Kip, N., Mersdorf, U., Barends, T. R. M., Jetten, M. S. M., Keltjens, J. T. & Kartal, B. (2016). *J. Biol. Chem.* **291**, 17077-17092.

Moser, C. C., Chobot, S. E., Page, C. C. & Dutton, P. L. (2008). *Biochim. Biophys. Acta – Bioenerg.* **1777**, 1032-1037.

Mowat, C. G., Rothery, E., Miles, C. S., McIver, L., Doherty, M. K., Drewette, K., Taylor, P., Walkinshaw, M. D., Chapman, S. K. & Reid, G. A. (2004). *Nat. Struct.Mol. Biol.* **11**, 1023–1024.

Murshudov, G. N., Skubak, P., Lebedev, A. A., Pannu, N. S., Steiner, R. A., Nicholls, R. A., Winn, M. D., Long, F. & Vagin, A. A. (2011). *Acta Cryst D* **67**, 355-367.

Oshiki, M., Ali, M., Shinyako-Hata, K., Satoh, H. & Okabe, S. (2016). *Environ. Microbiol.* **18**, 3133-3143.

Parey, K., Fielding, A. J., Sorgel, M., Rachel, R., Huber, H., Ziegler, C. & Rajendran, C. (2016). *FEBS J.* **283**, 3807-3820.

Polyakov, K. M., Boyko, K. M., Tikhonova, T. V., Slutsky, A., Antipov, A. N., Zvyagilskaya, R. A., Popov, A. N., Bourenkov, G. P., Lamzin, V. S. & Popov, V. O. (2009). *J. Mol. Biol.* **389**, 846–862.

Sam, K. A., Fairhurst, S. A., Thorneley, R. N. F., Allen, J. W. A. & Ferguson, S. J. (2008). *J. Biol. Chem.* **283**, 12555–12563.

Schuck, P. (2000). *Biophys. J.* **78**, 1606-1619.

Shelnutt, J. A., Song, X. Z., Ma, J. G., Jia, S. L., Jentzen, W. & Medforth, C. J. (1998). *Chem. Soc. Rev. (Chemical Society Reviews)* **27**, 31–41.

Sievers, F., Wilm, A., Dineen, D., Gibson, T. J., Karplus, K., Li, W. Z., Lopez, R., McWilliam, H., Remmert, M., Soding, J., Thompson, J. D. & Higgins, D. G. (2011). *Mol. Syst. Biol.* **7**.

Simon, J., Kern, M., Hermann, B., Einsle, O. & Butt, J. N. (2011). *Biochemic. Soc. Trans.* **39**, 1864-1870.

Strous, M., Pelletier, E., Mangenot, S., Rattei, T., Lehner, A., Taylor, M. W., Horn, M., Daims, H., Bartol-Mavel, D., Wincker, P., Barbe, V., Fonknechten, N., Vallenet, D., Segurens, B., Schenowitz-Truong, C., Medigue, C., Collingro, A., Snel, B., Dutilh, B. E., Op den Camp, H. J. M., van der Drift, C., Cirpus, I., van de Pas-Schoonen, K. T., Harhangi, H. R., van Niftrik, L., Schmid, M., Keltjens, J., van de Vossenberg, J., Kartal, B., Meier, H., Frishman, D., Huynen, M. A., Mewes, H. W., Weissenbach, J., Jetten, M. S. M., Wagner, M. & Le Paslier, D. (2006). *Nature* **440**, 790–794.

Tikhonova, T. V., Slutsky, A., Antipov, A. N., Boyko, K. M., Polyakov, K. M., Sorokin, D. Y., Zvyagilskaya, R. A. & Popov, V. O. (2006). *Biochim. Biophys. Acta – Prot. Proteom.* **1764**, 715-723.

van de Vossenberg, J., Woebken, D., Maalcke, W. J., Wessels, H. J. C. T., Dutilh, B. E., Kartal, B., Janssen-Megens, E. M., Roeselers, G., Yan, J., Speth, D., Gloerich, J., Geerts, W., van der Biezen, E., Pluk, W., Francoijs, K. J., Russ, L., Lam, P., Malfatti, S. A., Tringe, S. G., Haaijer, S. C. M., Op den Camp, H. J. M., Stunnenberg, H. G., Amann, R., Kuypers, M. M. M. & Jetten, M. S. M. (2013). *Environ. Microbiol.* **15**, 1275-1289.

Vonrhein, C., Blanc, E., Roversi, P. & Bricogne, G. (2007). *Meth. Mol. Biol.* **364**, 215-230.

Table 1 Data collection and processing

Values for the outer shell are given in parentheses.

	Fe-peak dataset	Native (6H5L)
Diffraction source	SLS PX-II	Rigaku 007-HF
Wavelength (Å)	1.700	1.5418
Temperature (K)	100	100
Detector	Pilatus 6M	MAR345 image plate
Crystal-detector distance (mm)	300	250
Rotation range per image (°)	0.25	0.25
Total rotation range (°)	720	46.5
Exposure time per image (s)	0.25	600
Space group and setting used	*R*32, hexagonal	*R*32, hexagonal
a, *b*, *c* (Å)	138.6, 138.6, 264.4	140.2, 140.2, 262.1
α, β, γ (°)	90, 90, 120	90, 90, 120
Mosaicity (°)	0.20	0.17
Resolution range (Å)	110-3.7 (3.8-3.7)	60-2.6 (2.7-2.6)
Total No. of reflections	416,481 (30,336)	84,176 (4,707) #
No. of unique reflections	20,235 (1,558)	29,065 (1,879) #
Completeness (%)	100.0 (100.0)	94.4 (84.5) #
Redundancy	20.6 (19.5)	2.9 (2.5) #
$\langle I/\sigma(I) \rangle$	35.8 (17.2)	10.6 (3.4) #
R_{meas}	0.091 (0.247)	0.113 (0.393) #
Overall *B* factor from Wilson plot (Å^2)	49.4	35.1

Treating Friedel mates as identical reflections

Table 2 Refinement

Values for the outer shell are given in parentheses.

Resolution range (Å)	60-2.6
Completeness (%)	94.4
σ cutoff	None
No. of reflections, working set	27,596
No. of reflections, test set	1,469
Final R_{cryst}	0.1894
Final R_{free}	0.2336
ML-based coordinate error (Å)	0.33
No. of non-H atoms	6,471
Protein	4,107 (chain A) 1,737 (chain B)
Ion	-
Ligand	430 (10 hemes)
Water	197
Total	6,471
R.m.s. deviations	
Bonds (Å)	0.003
Angles (°)	0.712
Average *B* factors (Å^2)	
Protein	28.9 (chain A) 38.1 (chain B)
Ion	-
Ligand	24.2 (hemes)
Water	29.8
Ramachandran plot	
Most favoured (%)	97.2
Allowed (%)	2.5
Disallowed (%)	0.3

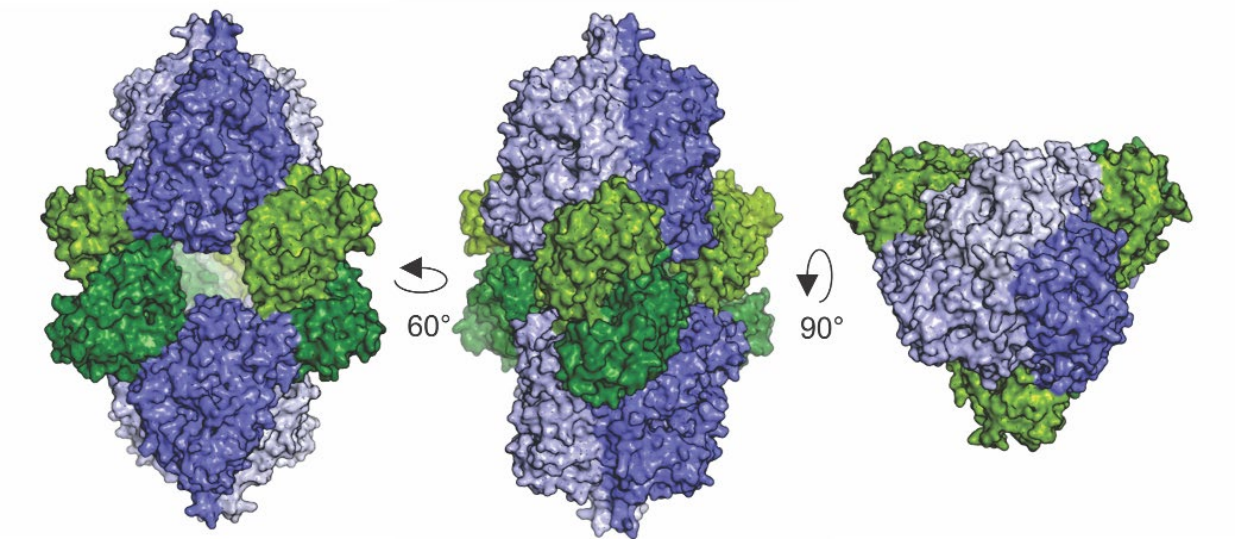

Figure 1 Overall structure of the KsHAOr-DH complex. The KsHAOr-DH heterododecamer is rendered as surface representation. In the left panel two side-views are depicted, in the right panel a view of the upper half of the heterododecamer from the top. The two KsHAOr trimers are coloured in different shades of blue while the six KsDH molecules arranged in the equatorial ring are shown in different shades of green. All structural figures were prepared using PyMol (DeLano, 2002).

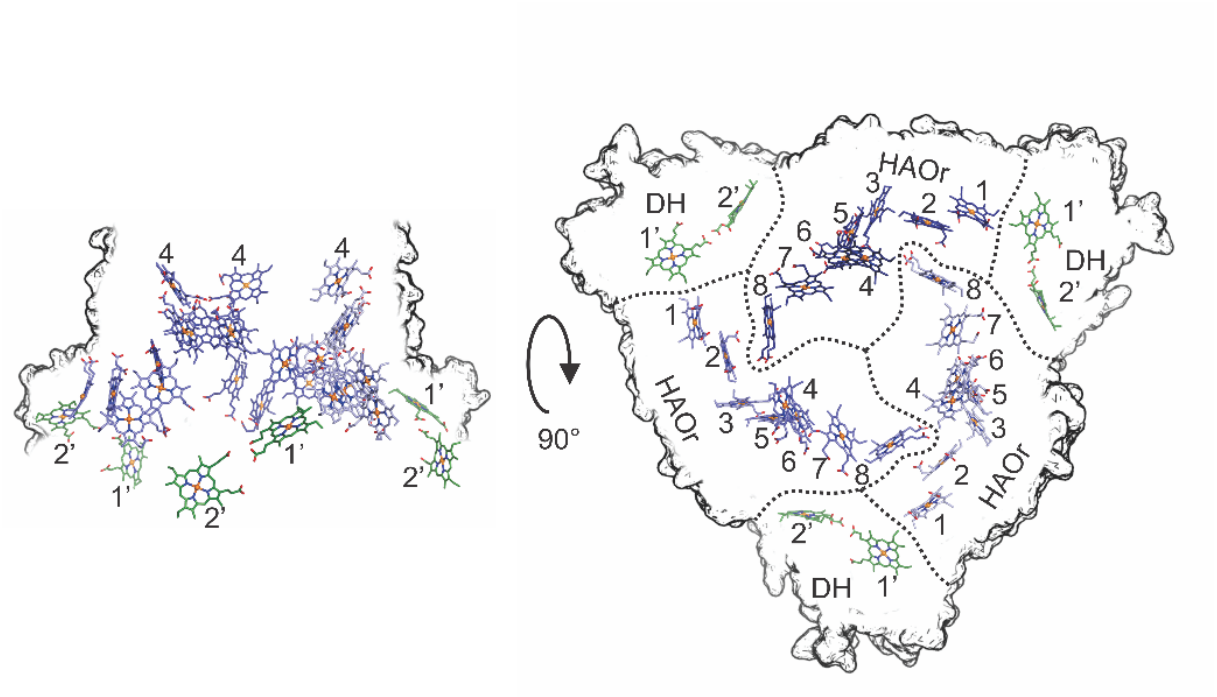

Figure 2 Arrangement of the hemes in the KsHAOr-DH heterododecamer. Only the upper half of the complex is depicted, containing 30 hemes, which are arranged as a three-armed spiral. The heme *c* cofactors bound to the N-terminal heme binding motif (heme 1') from each KsDH subunit are positioned next to heme 1 of KsHAOr at an edge-to-edge distance of 7.5 Å, *i.e.* a distance suitable for electron transfer through space. On the left panel a view from the side, on the right panel a view from the top is shown.

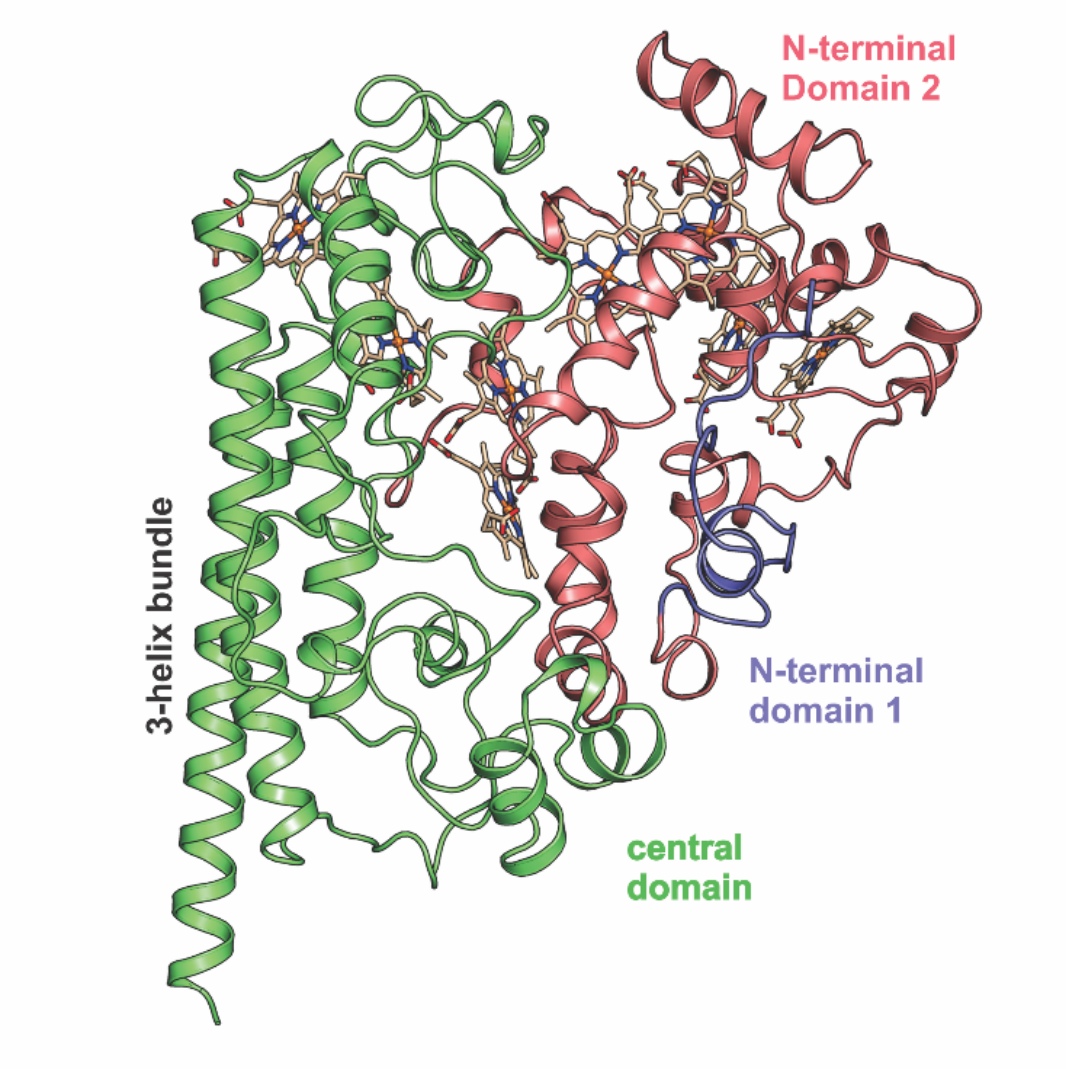

Figure 3 Structural details of the KsHAOr monomer. The KsHAOr monomer can be divided into three domains as indicated in figure 3: an N-terminal domain 1 (blue), an N-terminal domain 2 (red) and a central domain (green) as originally described for NeHAO (Igarashi *et al.*, 1997). The secondary structure elements of the protein are rendered as cartoon, the heme cofactors as stick models.

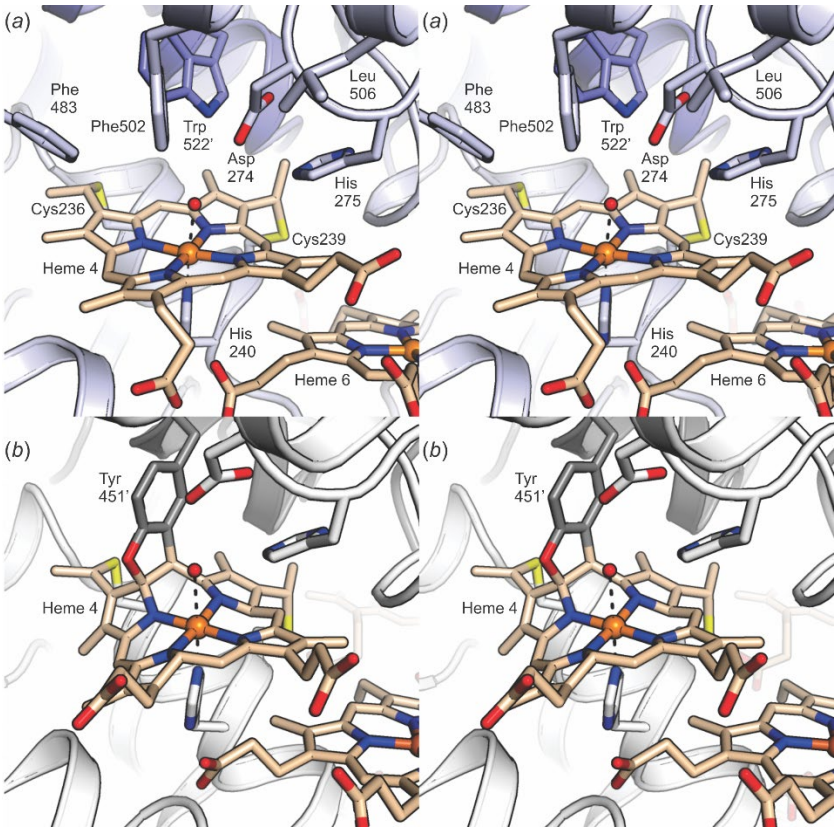

Figure 4 KsHAOr active site structure. (*a*). Stereo view of the KsHAOr active site. Secondary structure elements in the environment of heme 4 are shown as cartoons; the water molecule bound to the heme iron is shown as a red sphere. Heme 4 as well as the side chains of important residues in its environment are shown as stick models. The heme binding motif ($C^{236}DMC^{239}H^{240}$), the conserved Asp-His pair (Asp274 and His275) as well as Trp522' as part of the WWW motif are depicted. The carbon atoms in one subunit are shown in light blue, those in the adjacent subunit are rendered in dark blue. (*b*). Stereo view of the active site of KsHOX (pdb id 4N4J, (Maalcke *et al.*, 2014)), showing the pronounced ruffling of heme 4 caused by the covalent links to Tyr451'. In KsHAOr (panel *a*), the deformation of heme 4 is considerably less pronounced than in KsHOX, and appears to be more a bending than a ruffling of the heme plane.

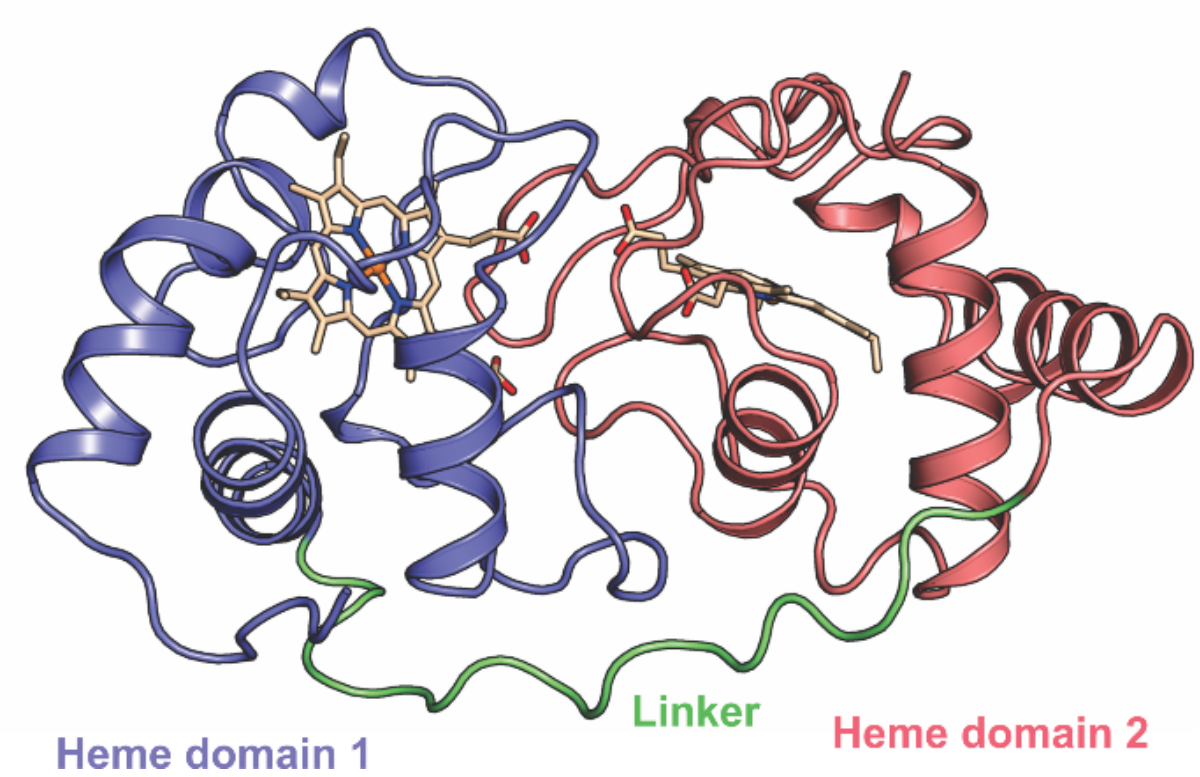

Figure 5 Structural details of the diheme cytochrome *c* KsDH. The diheme cytochrome *c* KsDH consists of two class I cytochrome *c* domains (N-terminal heme domain 1 in blue, C-terminal heme domain 2 in red) connected by a flexible linker (green) based on the sequence annotation used in figure S5. In each cytochrome domain, the hemes are coordinated by proximal histidines (His57 and His176) and distal methionines (Met112 and Met230). The secondary structure elements of the protein are rendered as cartoon, the heme cofactors as stick models.

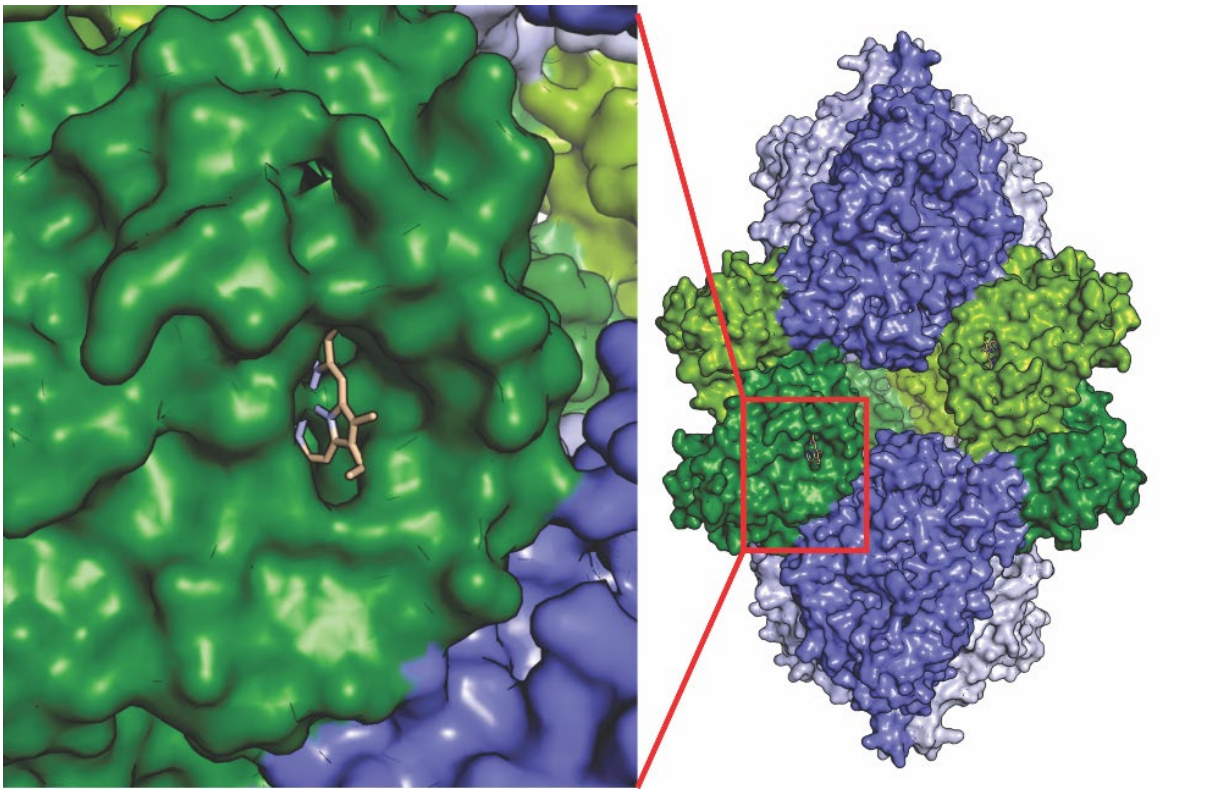

Figure 6 Location of heme 2’ of KsDH on the surface of the complex. Another heme 2’ moiety can be seen on the right side, inside the light green KsDH molecule opposite the hole in the side of the complex.

Supporting information

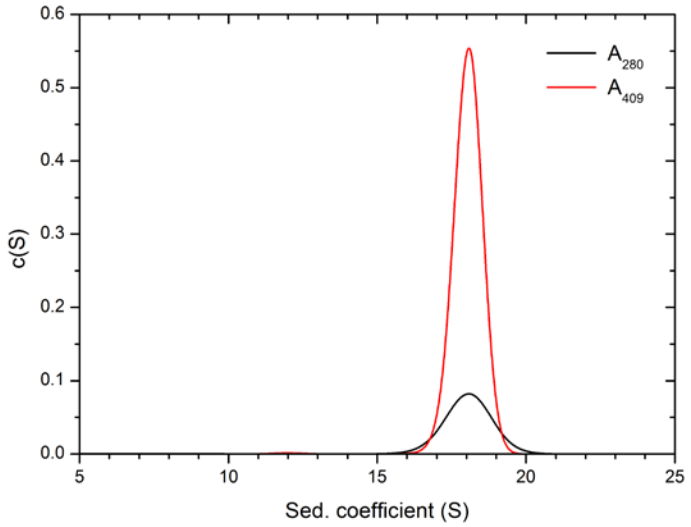

Figure S1 Sedimentation coefficient distribution of KsHAOr-DH

A sample of *K. stuttgartiensis* HAOr-DH was diluted to $A_{280}^{1\ cm}$=0.22, $A_{409}^{1\ cm}$=0.65 and analyzed by analytical ultracentrifugation in the sedimentation velocity (SV) mode at 20,000 rpm in a buffer containing 25 mM KCl, 25 mM HEPES/KOH, pH 7.5 at 20 °C. Absorption scan data were recorded at 280 nm (black curve) and 409 nm (red curve).

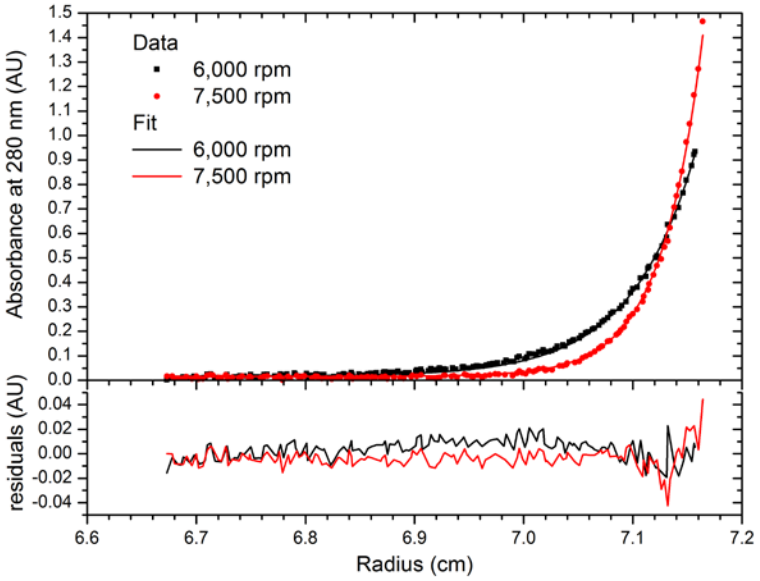

Figure S2 Sedimentation equilibrium analytical ultracentrifugation of KsHAOr-DH

Sedimentation equilibrium curves of KsHAOr-DH after 22 h equilibration at 6,000 rpm (black) and 7,500 rpm (red) at 20 °C. The data points were averaged from five individual scans at 280 nm and globally fitted assuming a model of discrete non-interacting species in SEDPHAT which resulted in a molecular mass of 545,974 Da (calculated 545,883 Da).

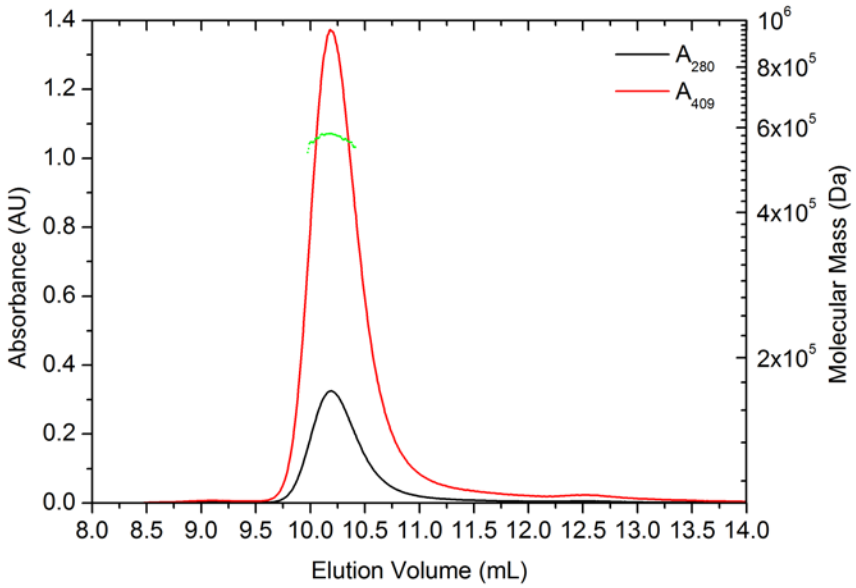

Figure S3 Size exclusion chromatogram and molar mass distribution of KsHAOr-DH

A sample of *K. stuttgartiensis* HAOr-DH (approximately 180 µg, re-purified by gel filtration) was separated on a Superdex 200 increase (10/300 GL) gel filtration column (GE Healthcare, Uppsala, Sweden) at room temperature in a buffer containing 150 mM KCl, 50 mM HEPES/KOH, pH 7.5. The absorbance traces at 280 nm (black) and 409 nm (red) as well as the molar mass distribution determined by multi-angle static light scattering (green) are indicated.

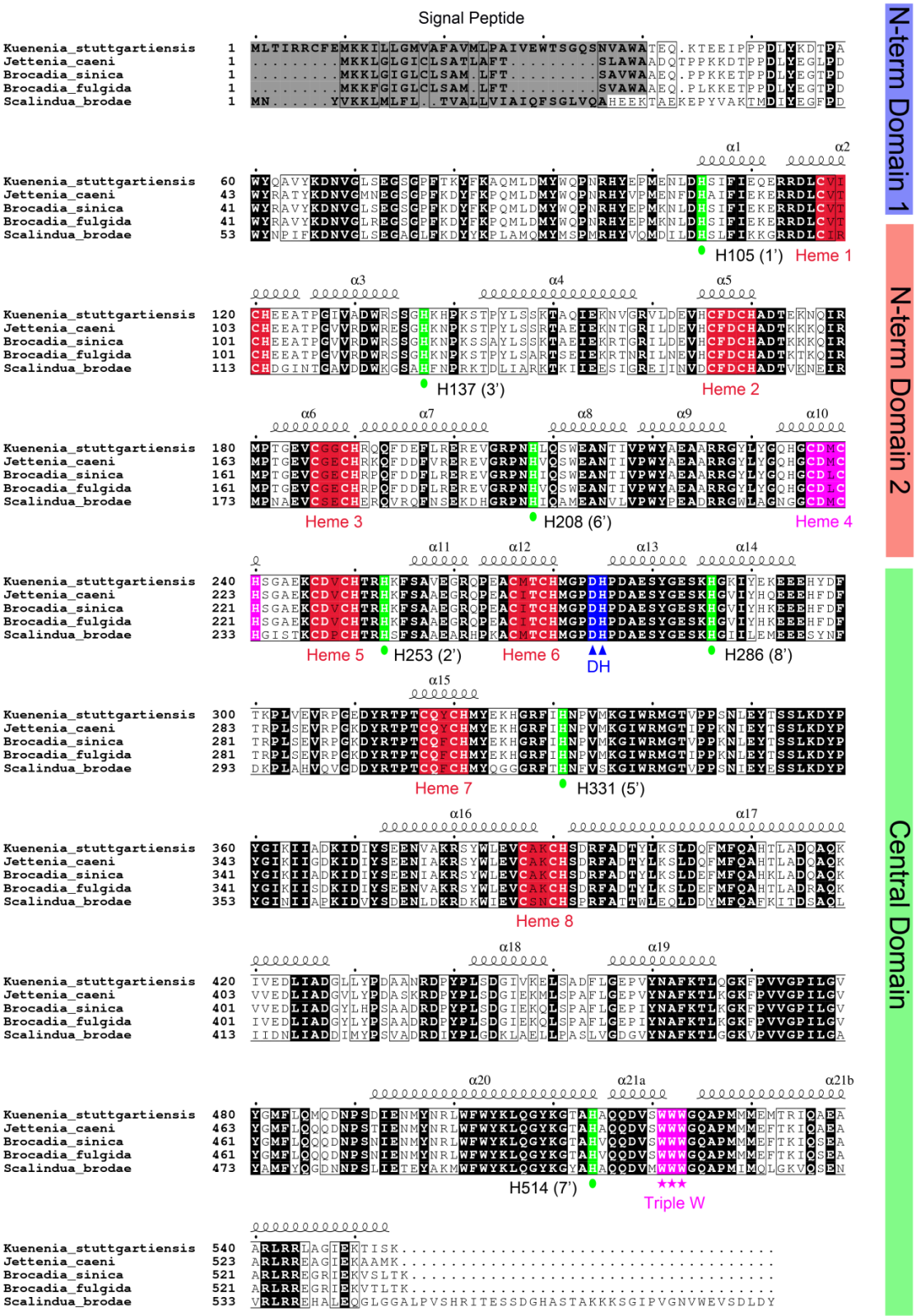
Signal Peptide
N-term Domain 1
N-term Domain 2
Central Domain
Kuenenia_stuttgartiensis
Jettenia_caeni
Brocadia_sinica
Brocadia_fulgida
Scalindua_brodae
α1
α2
α3
α4
α5
α6
α7
α8
α9
α10
α11
α12
α13
α14
α15
α16
α17
α18
α19
α20
α21a
α21b
H105 (1')
Heme 1
H137 (3')
Heme 2
Heme 3
H208 (6')
Heme 4
Heme 5
H253 (2')
Heme 6
DH
H286 (8')
Heme 7
H331 (5')
Heme 8
H514 (7')
Triple W

Figure S4 Sequence alignments of KsHAOr homologues (previous page). The sequence of *Kuenenia stuttgartiensis* HAOr (kustc0458, CAJ71203.1) was aligned to its orthologues from *Jettenia caeni* (KSU1_C0839, WP_007221541.1), *Brocadia sinica* JPN1 (BROSI_A0131, WP_052561403.1), *Brocadia fulgida* (BROFUL_02751, KKO18553.1) and *Scalindua brodae* (SCABRO_03687, KHE90580.1) using ClustalO (Sievers *et al.*, 2011). Secondary structure elements were manually assigned based on the structure of KsHAOr. *K. stuttgartiensis* HAOr shares 85 % sequence identity with its orthologues from *J. caeni* and *B. sinica*, 84 % with *B. fulgida* and 57 % with *S. brodae*. Fully conserved peptide sequences are marked black. The *c*-type heme binding motifs are highlighted in red, the active site heme in pink. The predicted signal peptides are highlighted in grey. The distal histidine ligands of the hemes (x', green circles), the conserved Asp-His pair (DH, blue triangles) and the triple tryptophan motif (pink stars) are also indicated. The figure was prepared using ESPript (Gouet *et al.*, 1999).

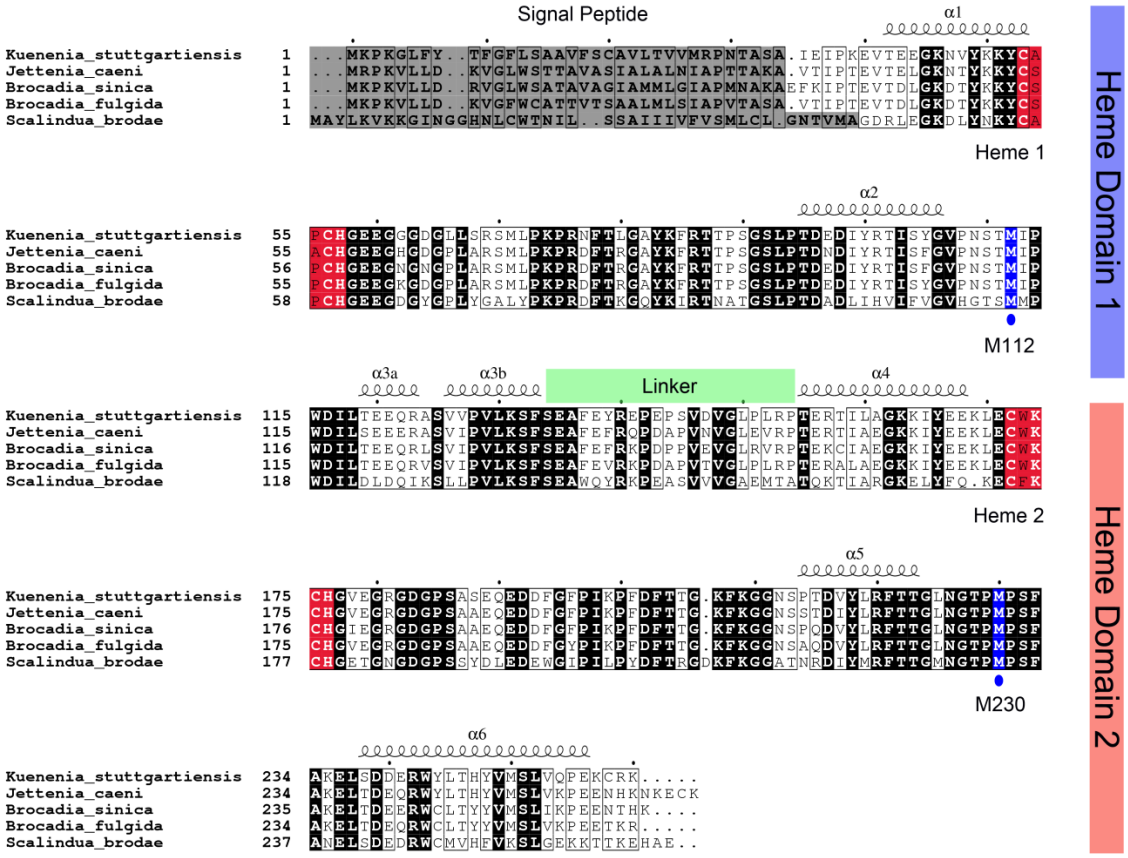

Figure S5 Sequence alignments of KsDH homologues. The sequence of *Kuenenia stuttgartiensis* diheme cytochrome *c* (KsDH, kustc0457, CAJ71202.1) was aligned to its orthologues from *Jettenia caeni* (KSU1_C0840, WP_007221542.1), *Brocadia sinica* JPN1 (BROSI_A0132, WP_052561405.1), *Brocadia fulgida* (BROFUL_02750, KKO18552.1) and *Scalindua brodae* (SCABRO_03686, KHE90579.1) using ClustalO (Sievers *et al.*, 2011). Secondary structure elements were manually assigned based on the structure of KsDH. *K. stuttgartiensis* diheme cytochrome *c* shares 77 % sequence identity with its orthologues from *J. caeni*, 75 % with *B. sinica*, 78 % with *B. fulgida* and 49 % with *S. brodae*. Fully conserved peptide sequences are marked black. The *c*-type heme binding motifs are highlighted in red. The predicted signal peptides are highlighted in grey. The two conserved methionine residues Met112 and Met230 serve as distal ligands to heme 1 and heme 2, respectively, and are marked with green circles. The figure was prepared using ESPript (Gouet *et al.*, 1999).